COMMUNICATIONS IN SCIENCE AND TECHNOLOGY
Homepage: cst.kipmi.or.id

One-stage microwave-assisted activated carbon preparation from Langsat peel raw material for adsorption of iron, manganese and copper from acid mining waste

Lailan Ni`mah, Sri Rachmania Juliastuti, Mahfud Mahfud*

Department of Chemical Engineering, Institut Teknologi Sepuluh Nopember, Surabaya 60111, Indonesia

Article history:
Received: 17 October 2023 / Received in revised form: 30 November 2023 / Accepted: 2 December 2023

Abstract

This study describes the efficacy of microwave technology for the preparation of an activated carbon from *Lansium domesticum* peel as an adsorbent to adsorb Fe, Cu, and Mn from acid mine waste. In contrast to the conventional pyrolytic carbonization technique, the described method demonstrated several unparalleled advantages, including superior energy efficiency and remarkably rapid processing. The reported microwave irradiation method was able readily to achieve a morphology and extensive surface area similar to that of a sample produced using the traditional pyrolytic carbonization method for 2 hours, and this was accomplished in just 10 minutes. The activated carbon obtained was characterized using SEM-EDX, BET-BJH, and proximate test and applied to adsorb metal ions from acid mine waste to evaluate the isothermal adsorption model. The best power for activated carbon production was 400 watts for 10 minutes, which met the requirements of ASTM D 4607 for determining the iodine value of activated carbon. Optimal mass for adsorbing Fe, Cu, and Mn from acid mine waste was 4 grams with the removal percentages of 94.08%, 83.69%, and 90.67%, respectively. BET surface area was 1367.0385 m^2/g along with a BJH cumulative volume and an average pore diameter of 1.112 cm^3/g and 2.25 nm, respectively. This suggests that it possesses mesoporous characteristics and adheres to the Langmuir model during the adsorption process, signifying monolayer adsorption. Meanwhile, kinetics followed the pseudo-second-order rate equation.

Keywords: Lansium Domesticum peel; microwave; activated carbon; adsorption; acid mine waste

1. Introduction

Langsat originates from the western part of Southeast Asia, ranging from the Thai Peninsula in the west to Kalimantan in the east (Indonesia). While mostly growing in the wild, in this region, Langsat has been naturalized and becomes one of the main fruits cultivated. In Kalimantan, it is found throughout the island. At a smaller scale, Langsat is also cultivated in Vietnam, Burma, India, Sri Lanka, Hawaii, Australia, Suriname, and Puerto Rico. In Indonesia, Langsat can be found in Banyuwangi, Palembang, Bangka, South and West Kalimantan, and in several regions in Sulawesi. This fruit has several edible parts, accounting for 68% of its weight. Per 100 g, it contains 84 g of water, small amounts of protein and fat, 14.2 g of carbohydrates, mainly reducing sugars, especially glucose, 0.8 g of fiber, 0.6 g of ash, 19 mg of Ca, 275 mg of K, some vitamins B1 and B2 but little vitamin C. The energy value is 238 kJ/100g [1].

Activated carbon mainly comprises free carbon with an amorphous or microcrystalline structure, obtained through a specialized treatment with high adsorption[2] properties. Carbon materials from plants, animals, or minerals can be used to produce activated carbon [3,4]. *Lansium domesticum* peel waste, which is harmful to the environment [5,6], can also be converted into activated carbon, as it is abundant in Borneo Island.

Chemical and physical methods are commonly used in manufacturing the activated carbon [7–9]. Nonetheless, due to numerous drawbacks associated with this approach, scientists have started a transition to the utilization of microwaves in the production of activated carbon, which offers several advantages [10] including higher heating rates, faster heating of the mixture and more uniform heat distribution. Indirect and selective heating allows for the enhanced control of the drying procedure, a reduction in equipment dimensions, and a decrease in waste generation [11,12]. Preliminary studies suggested that heat is transferred due to the interaction of dielectric molecules with microwaves [13]. Furthermore, the induced energy appears as heat through molecular friction, resulting in a more even distribution of heat and lower activation energy due to the high atomic mobility of the crystal structure [14]. This technique is non-contact, requiring lower activation temperatures and shorter processing times, resulting in energy conservation. Additionally, it generates a temperature gradient from the core to the external surface and leverages the thermal and catalytic effects of micro-plasmas, offering further advantages [15], It facilitates the effortless release of lighter

* Corresponding author.
Email: mahfud@chem-eng.its.ac.id
https://doi.org/10.21924/cst.8.2.2023.1299

components for the formation of additional pores, leading to improved efficiency, rapid initiation and termination, heightened safety, and reduced equipment size, requiring less preprocessing of the feedstock [16].

Numerous investigations have been carried out to explore the application of microwave heating for the removal [17] of dye waste. *Eupatorium adenophorum* materials, for instance, have been employed to produce activated carbon through a microwave-assisted KOH activation process, conducted at 700 W within a 15-minute duration. According to the BET-BJH characterization results, the calculated surface area, overall pore volume, and mean pore diameter were determined to be 3.918 m^2/g, 2.383 ml/g, and 2.43 nm [18].

Table 1. The previous research on activated carbon from biomass

Method	Surface Area	Ref.
Chemical-Microwave (2 stages), H_3PO_4 (4 hours, 110°C), 700 watts, 12.5 minutes	1552 m^2/g 1103 m^2/g	[19]
Method 1: Chemical - Physics (2 Stages), H_3PO_4 (12 hours, 110°C) Method 2: Carbonization - Chemical – Physics: 200°C, 30 minutes. Impregnated H_3PO_4 (12 hours, 110°C)	Iodine Number (mg/g): N_2: 896.48; CO2: 810.90 Steam: 973.70; Absent: 856.22 Iodine number N_2: 1021.74; CO_2: 1069.98 Steam: 902.40; Absent: 1040.58	[20]
Chemical (2 Stages), KOH and H_3PO_4 (1 hour, 1073 K), steam (1 hour, 1123 K)	1375 m^2/g for KOH; 466 m^2/g for H_3PO_4	[21]
Chemical – Physics (2 Stage): phosphoric (V) acid (24 hours, 30°C); Nitrogen (1 hour, 400°C); CO_2 (3 hours, 800°C	Nitrogen= 269.8-464.2 m^2/g. CO2=407.8-720.9 m^2/g	[22]
Physics – Chemical: Steam (878°C, 45 minutes); KOH (1 hour, 300°C)	Steam: 2541 m^2/g; CO_2:700 m^2/g	[23]
Chemical (2 stages): Carbonization (2 hours, 350°C); H_3PO_4 (30 minutes, 300°C)	Iodine Number FAC= 224,90 ± 0,50; CAC= 200,36 ± 0,30	[24]
Chemical (2 stages): H_3PO_4 and NaOH (24 hours, 105°C)	561.60 m^2/g, 265 m^2/g, 395.40 m^2/g	[25]
Physics- Chemical (2 Stages): HCl (12 hours, 378K)	1410 m^2/g	[26]
Chemical - Physics (2 stages): impregnation (323 K, 12 hours)	1347 m^2/g	[27]
Chemical - Physics (2 Stages): $ZnCl_2$ (12 hours, 120°C) and Carbonization (500°C, 3 hours)	1213 m^2 /g	[28]
Chemical - Physics (2 stages): ZnCl2 (24 hours), nitrogen (1 hour, 650° C)	995.799 m^2/g	[29]

Acid mine water originates from the geochemical reaction of exposed sulfide minerals interacting with water and air. It poses a serious environmental problem for containing the high levels of heavy metals and sulfate metals such as iron, manganese, copper, cadmium, lead, and nickel. The elevated metal and acid content in acid mine water can contaminate surface water, groundwater, and soil, potentially causing harm to plants, and negatively impacting wildlife, aquatic species, and humans[30].

This study in turn aims to produce short-time and low-cost activated carbon from *Lansium domesticum* peel (ACLDP) and investigate its efficacy in adsorbing metal contents in acid mine water. Specific aims include establishing a method for production and characterization using microwave radiation, evaluating efficiency as an adsorbent, investigating adsorption isotherms, and kinetics adsorption. It also investigate *Lansium domesticum* peel as an eco-friendly source of activated carbon.

2. Materials and Methods

This study was structured into two distinct phases. In the initial phase, tasks encompassed carbonization processes, the production of activated carbon, and the subsequent assessment of the quality of the resulting products. During the second phase, the focus shifted to apply activated carbon derived from agricultural waste to eliminate heavy metal[31]ad pollutants, specifically iron (Fe^{3+}), manganese (Mn^{2+}), and copper (Cu^{2+}) from acidic mine water. It is important to note that in this study, artificial waste was generated using $FeSO_4$ for iron, MnO_2 for manganese, and $CuSO_4$ for copper. The artificial waste conditions were adjusted to match the acidic mine water conditions from PT. Jorong Barutama Greston (PT. JBG) located in Batulicin, South Kalimantan, namely Fe 127.20 ppm, Mn 37 ppm, and Cu 25.61 ppm [32].

2.1. Materials and equipment

The raw material for producing activated carbon was *Lansium domesticum* peel obtained from South Kalimantan. The solutions of $FeSO_4$, MnO_2, and $CuSO_4$ used for activated carbon applications were purchased from Merck. The necessary apparatus for producing activated carbon included a crusher, an oven dryer (specifically the Memmeth DIN 12880-KI model), a microwave (Sharp R 728(S) IN), an analytical balance (Shimadzu AW-220), and an 850-micron filter. During the implementation stage, additional equipment was required, including a Microwave Sharp R 728(S) IN for producing activated carbon from agricultural waste, SEM-EDX JEOL JSM-6360LA, and BET-BJH Micromeritics TriStar II 3020 for characterizing the activated carbon. Common laboratory equipment such as analytical balances, porcelain dishes, desiccators, furnaces, ovens, and various types of laboratory glassware are employed as well.

2.2. The activated carbon manufacturing process

subjected to microwave treatment at three different power levels: 400 watts, 500 watts, and 600 watts with a duration of 10 minutes on each. The adsorbent used was technical activated carbon with an amount of 10% by weight of the mass to be made in the microwave[33]. Prior to conduct the process, flushing was firstly carried out using nitrogen gas to prevent the

occurrence of the oxidation during the process.

2.3. Utilizing activated carbon for acid mine waste remediation and assessing adsorption isotherms

To treat acid mine wastewater, activated carbon meeting the required standards was employed as an adsorbent. The experiment utilized both model aqueous solutions and real effluent containing Fe, Cu, and Mn in liquid waste. Two Erlenmeyer flasks were employed to blend 2-7 grams of the adsorbent with a 100 mL sample containing 127.20 ppm FeSO4, 37.00 ppm MnO2, and 25.61 ppm CuSO4. Following a 60-minute agitation period using a rotary shaker set at 50 rpm, the mixture was subsequently filtered through Whatman 42 filter paper. The concentration of metal ions in the filtrate was quantified before and after treatment using atomic absorption spectrophotometry in which the results were expressed in mg/g. The adsorption isotherm model was established based upon this data.

The standards of SNI 6989.4:2009, SNI 6989.5:2009, and SNI 6989.6:2009 were utilized in the spectrophotometric analysis to ascertain the overall concentrations of Fe, Mn, and Cu. Subsequently, the post-treatment concentrations of FeSO4, MnO2, and CuSO4 were employed in calculating the adsorption capacity and constructing the adsorption isotherm model, employing both the Langmuir and Freundlich equations [34].

The equation was employed to determine the quantity of adsorbed Fe, Cu, and Mn ions (Q_e) for each experimental run:

$$Q_e = \frac{(C_0 - C_e)V}{W} \quad (1)$$

In this equation:
Q_e (mg/g) represents the adsorption capacity,
C_0 (mg/L) denotes the initial concentrations of Fe, Cu, and Mn,
C_e (mg/L) stands for the equilibrium concentrations of Fe, Cu, and Mn,
V (L) signifies the volume of the acidic mine water, and
W (g) represents the weight of the applied adsorbent[35].

Equation (2) symbolizes the condition of the Langmuir isotherm model.

$$\boldsymbol{q = q_{max}\left(K_L \frac{C_e}{1+K_L C_e}\right)} \quad (2)$$

Within this equation, q (mg/g) represents the concentration of adsorbed heavy metal particles per unit mass of the beads, K_L signifies the Langmuir equilibrium constant associated with the binding site affinity, C_e denotes the equilibrium concentration of Ni^{2+} ions, and q_{max} is the theoretical maximum monolayer saturation capacity [36].

The Freundlich isotherm model illustrates that adsorption occurs on a heterogeneous surface, leading to an observable state[36]:

$$q_e = K_F C_e^{1/n} \quad (3)$$

Here, q_e represents the adsorption capacity (mg/g), C_e signifies the adsorbent concentration in the solution (mg/L), while K_F and n are the empirical constants describing the adsorption capacity and the intensity of the process, respectively.

3. Results and Discussion

3.1. Assessment of activated carbon quality using proximate analysis results

Proximate analysis serves to determine water content, ash level, flammable matter, fixed carbon, and iodine number. It is an analysis that classifies the components contained in materials based on their chemical composition and function.

Table 2 displays the proximate analysis results of activated carbon produced from agricultural waste under the authorization of 400 watts using a Microwave.

Table 2. Results of the proximate analysis for activated carbon

Parameter	Unit	Result
Water content	%	8.08
Ash level	%	4.03
Flammable matter	%	6.61
Fixed carbon	%	75.57
Iodine number	g Iod/100 g	850.91

To determine the amount of water that can evaporate, it is essential to assess the water content. The loss of water molecules in activated carbon contributes to the expansion of pores. The larger pores lead to an increased surface area for the activated carbon. Nonetheless, it is worth noting that elevated water content can influence the carbon's hygroscopic characteristics. In our research, the water content was determined to be 8.08%. We also conducted ash analysis to detect the presence of metal oxides in the activated carbon, which consisted of overlapping layers forming the pores. Sites in the pores often contain impurities in the form of inorganic minerals and metal oxides that cover the pores [37].

During the activation process, impurities also evaporate, causing the pores to open. This then leads to an expanded surface area of the activated carbon [38]. The ash level is assumed to be the mineral residue left over from carbonization because the natural material from which carbon made is not only carbon compounds but also minerals, some of which are lost during carbonization, some of which are expected to remain in the carbon. The ash level greatly affects the quality of the carbon produced [39]. Excessive ash content can potentially obstruct the pores within the carbon, leading to a reduction in the carbon's surface area [39]. The assessment of flammable substance levels is conducted to gauge the quantity of remaining substances within the activated carbon [40]. The use of chemicals as the activators causes the contamination of the carbon obtained [41]. In general, activators leave residues, such as water-insoluble oxides, when washed off.

The flammable matter substances meet the established standards. Certainly, the elevated activation temperature results in the full decomposition of compounds such as CO_2, CO, CH, and H_2. The ash level in this study obtained a result of 4.03%. Based on the calculation results, the flammable matter content was 6.61%; thus, it can be considered to have met the SNI standard for a maximum ash level of 25% activated carbon. Carbon that has been fixed was analyzed to determine the pure carbon content after carbonization and activation. The value of the fixed carbon based on SNI is at least 65% for the powdered activated carbon. In this study, the carbon content bound to the activated carbon of Langsat peel was 75.57%. The carbon's size is impacted by the presence of flammable matter and ash levels.

Moreover, the composition of cellulose and lignin in the raw material also has an effect on the carbon. The low carbon can be determined by the large amount of carbon that reacts with water vapor to produce CO and CO_2.

The assessment of iodine adsorption capacity serves as a fundamental criterion for evaluating the quality of activated carbon, providing insights into its capability to absorb smaller molecules. A higher quantity of iodine generated signifies that the activated carbon exhibits stronger adsorption properties, indicating the presence of a greater number of pores. According to [42], The moisture content in activated carbon is affected by some factors such as the carbon's inherent hygroscopic characteristics, humidity in environment, and duration of the cooling, grinding, and sieving procedures. The ash content of activated carbon is typically influenced by research methodologies, including the activated carbon cleaning process. On the other hand, the presence of flammable substances in activated carbon is linked to the quantity of nitrogen and sulfur compounds that undergo combustion[43]. The immobilized carbon is a consequence of the elevated ash content present in the activated carbon. According to[44], a good carbon as a raw material for activated carbon ranges from 70-80%.

The adsorption capacity of activated carbon toward iodine solution serves as an indicator of its capability to adsorb substances with low molecular weight. The presence of a high ash level can result in the coverage of numerous pores within the activated carbon with ash, which has an impact on its iodine absorption capacity. The adsorption capacity of activated carbon for iodine correlates with its surface area where a higher iodine number signifies a greater capacity to adsorb the adsorbates or solutes. The Iodine number test is conducted to assess the activated carbon's ability to adsorb molecules with small diameters, and a higher iodine number implies a stronger capacity to adsorb the adsorbates or solvents [45]. According to the proximate test outcomes, the quality of the carbon derived from agricultural waste sourced from *Lansium domesticum* peel conforms to the specifications outlined in SNI 06-3730-1995 for technical-grade carbon and ASTM D 4607 for determining the iodine value of activated carbon, making it suitable for direct application in the adsorption process of acid mining waste.

3.2. Analysis of the surface morphology and composition of activated carbon produced from Lansium domesticum peel

The synthesized material was characterized by its crystal morphological structure, particle size and element distribution using the SEM-EDX instrument. Figure 1, 2, and 3 depict the findings regarding the surface topography and elemental composition analysis of agricultural waste, carbon, and activated carbon derived from agricultural waste (*Lansium domesticum* peel).

Figures 1, 2, and 3 illustrate the results derived from SEM-EDX (Scanning Electron Microscopy-Energy Dispersive X-Ray) analysis. The outcomes revealed that the activated carbon produced from agricultural waste, specifically *Lansium domesticum* peel, using a microwave at 400 watts yielded a carbon content of 75.79%. Notably, the activated carbon generated at 400 watts showcases a more prominent, cleaner, and pore-forming structure compared to those produced at 500 and 600 watts. Consequently, the 400-watt power setting was chosen due to its capacity to achieve the complete decomposition of cellulose and lignin at high temperatures [46,47].

The generation of activated carbon is significantly affected by microwave power. An increase in microwave power can cause the temperature to rise, enhancing the activation process and producing more pores [48].

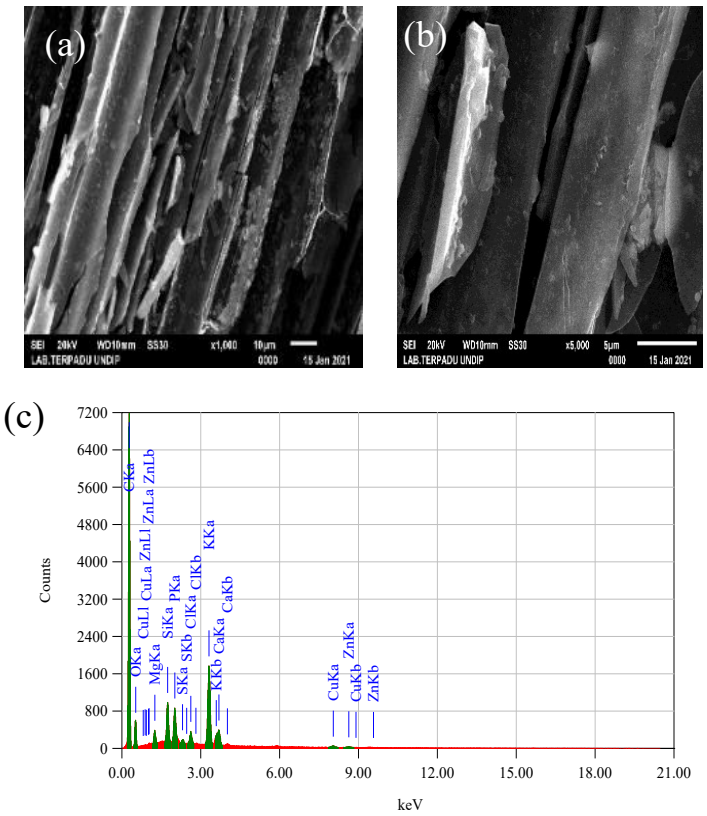

Fig. 1. (a) SEM micrographs of ACLDP at 400 watts power x1000 and (b) x5000 magnification (c) EDX contents composition of ACLDP at 400 watts power

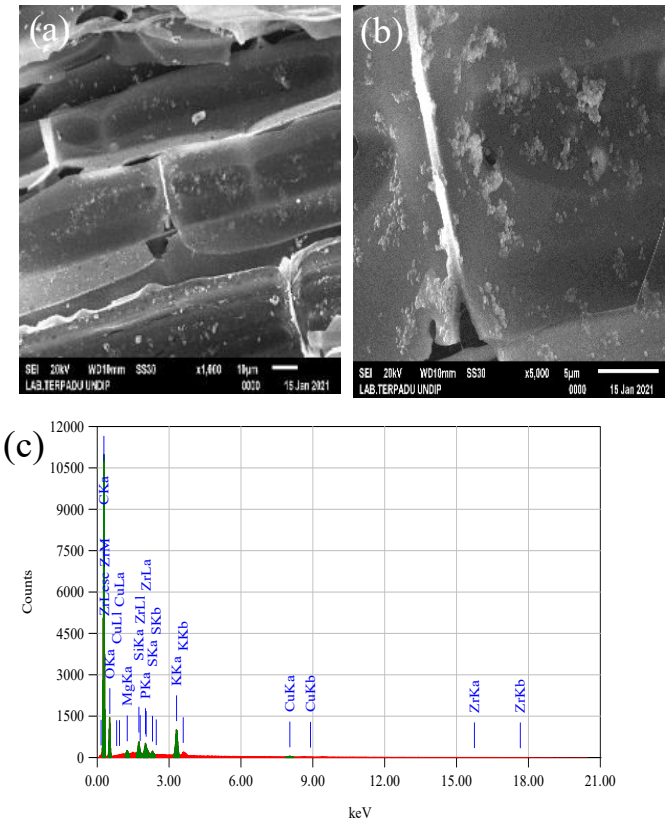

Fig. 2. (a) SEM micrographs of ACLDP at 500 watts power x1000 and (b) x5000 magnification (c) EDX contents composition of ACLDP at 500 watts power

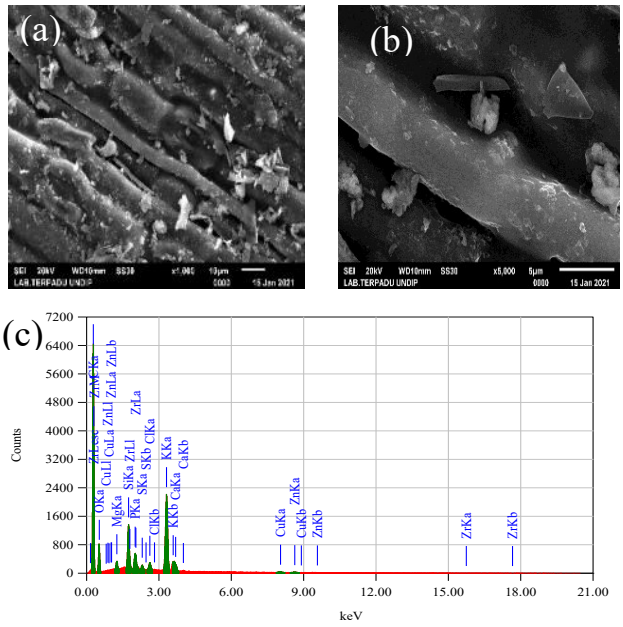

Fig. 3. (a) SEM micrographs of ACLDP at 600 watts power x1000 and (b) x5000 magnification (c) EDX contents composition of ACLDP at 600 watts power

Nevertheless, excessive power has the potential to incinerate a portion of the carbon, alter the pore structure, and reduce adsorption capacity, ultimately resulting in a decline in carbon adsorption performance [49]. As per [50], the microwave power determines the temperature of the raw material. Higher microwave power corresponds to elevated temperatures, facilitating the acceleration of activated carbon formation. Augmenting the microwave power causes the raw material to absorb more energy, expediting pore formation and diminishing the percentage yield. Nevertheless, excessive heating or overheating may result in the production of subpar activated carbon due to the potential reduction of mesopores and micropores in the activated carbon [51].

Based on the research conducted by [18], with the increased microwave radiation power, a higher temperature was generated, causing more non-carbon materials to evaporate. Here, the microwave power level directly influenced the temperature of the raw materials; higher microwave power resulted in the elevated temperatures that could expedite the reaction rate in the formation of activated carbon. The increase in microwave power causes the raw material to receive more energy, which will accelerate the formation of pores in the raw material and reduce the yield percentage produced. However, excessive heating (overheating) will produce activated carbon, which is not good as it can reduce mesopores and micropores in the activated carbon [52]. Findings from other research indicated that as the carbonization temperature rises, the yield of activated carbon tends to decrease, whereas the analysis of fixed carbon content increases [53].

EDX analysis was conducted to identify the components or atomic composition of the activated carbon derived from *Lansium domesticum* peel at three different power levels: 400 watts, 500 watts, and 600 watts. Table 3 presents the outcomes of the EDX Analysis.

Table 3 shows the findings of the EDX analysis conducted on activated carbon derived from Lansium domesticum peel. It can be observed that the constituents of activated carbon produced from Lansium domesticum peel included the elements of C, O, Mg, Si, P, S, Cl, K, Ca, Cu, Zn, and Zr. The highest composition was found in carbon and oxygen. The findings obtained from preparing activated carbon from the agricultural waste of Lansium domesticum peel using a microwave at 400 watts of power showed 75.79% carbon, greater than that of at 500 watts or 600 watts.

Table 3. EDX adsorbent analysis results

Element	Mass %		
	400 watts	500 watts	600 watts
Carbon	75.79	73.47	70.55
Oxygen	14.11	22.56	18.24
Magnesium	0.49	0.18	0.40
Silicon	1.31	0.54	1.90
Phosphorus	1.39	0.36	0.79
Sulphur	0.19	0.16	0.25
Chlorine	0.49	-	0.42
Potassium	4.56	1.95	5.78
Calcium	0.88	-	0.54
Copper	0.49	0.37	0.33
Zinc	0.32	-	0.31
Zirconium	-	0.40	0.50

3.3. Surface area and pore size distribution of activated carbon from Lansium domesticum peel (ACLDP)

The results obtained through BET (Brunauer-Emmett-Teller) and BJH (Barrett-Joyner-Halenda) tests revealed valuable insights into the properties of the carbon derived from *Lansium domesticum* peel waste and the activated carbon produced from it. Specifically, the carbon from *Lansium domesticum* peel waste exhibited a BET surface area of 759.0899 m2/g. Furthermore, the BJH adsorption analysis indicated a cumulative volume of pores within the range of 1.7000 nm to 300.0000 nm, measuring 0.598 cm3/g with an average pore diameter (4V/A) of 2.09 nm. On the other hand, the activated carbon generated from *Lansium domesticum* peel waste showed a notably higher BET surface area, measuring 1367.0385 m2/g. The BJH adsorption analysis for this activated carbon revealed a cumulative pore volume within the size range of 1.7000 nm to 300,0000 nm, equaling 1,112 cm3/g, along with an average pore diameter (4V/A) of 2.25 nm. These results provide valuable information about the porous structure and surface area characteristics of the two types of carbon materials. Based on these findings, the waste had pore diameters ranging from 2 to 50 nm similar to research conducted by[54]. The paragraph describes the utilization of microwaves for creating activated carbon from palm kernel shells. This process involves a modified household microwave, equipped with a quartz reactor and paired with a PID temperature controller. The most effective conditions in producing activated carbon were determined to be at the temperature of 900°C and an irradiation time of 40 minutes. These conditions yielded activated carbon with specific properties, including a BET surface area of 571.37 m^2/g, a total pore volume of 0.244 cm^3/g, and a micropore volume of 0.198 cm^3/g. In the study conducted by [55], it also suggested the advantages of using a microwave in activating the activated carbon. The study involved the utilization of microwave assistance for the activation of carbon derived from palm oil waste. The findings of the research showed that the highest recorded surface area reached 1256 m^2/g. The research also determined an average pore diameter of 1.010 cc/g, equivalent to an average pore diameter of 32.4 Å.

The use of heat and microwaves to accelerate the carbonization and activation process of carbon can be observed in the graph showing the heating before and after activation, as well as the increase in temperature and the time required for heating.

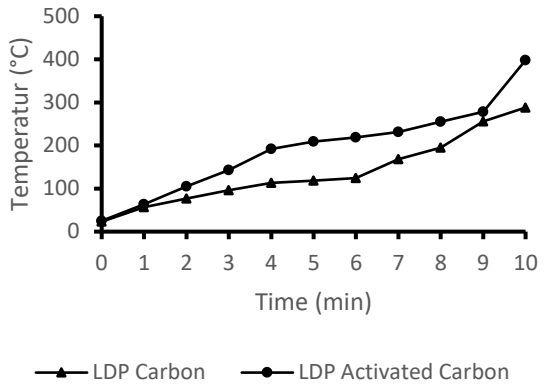

Fig. 4. Temperature Profile using Microwave

As depicted in Figure 4, employing microwaves for the carbonization and activation processes of activated carbon offers advantages in comparison to traditional heating methods. The introduction of the temperature controller allowed for the precise and efficient control of heating rates, as well as the carbonization and activation temperatures. The findings from the study revealed that temperature and irradiation time played a substantial role in shaping the porosity of the activated carbon, while having minimal to no effect on the actual yield of activated carbon. Moreover, the use of microwave heating was found to promote the creation of activated carbon with a greater surface area and favorable porosity characteristics [56].

3.4. Bio adsorbent mass dosage effect

Figure-1, 2, and 3 show the spectrophotometric (AAS) results of activated carbon made from Langsat fruit for adsorbing Fe, Mn, and Cu metal contents from acid mine waste. The maximum metal removal of 96.44%, 98.16%, and 82.21% was recorded for Mn, Fe, and Cu metals treated with activated carbon. Due to its adsorbent properties, the peak values were observed at an optimal dosage of 4 grams, beyond which they stabilized and did not show further variations [36]. The initial pH of the waste was 4-5. When the adsorption process occurred, it became 5-6.

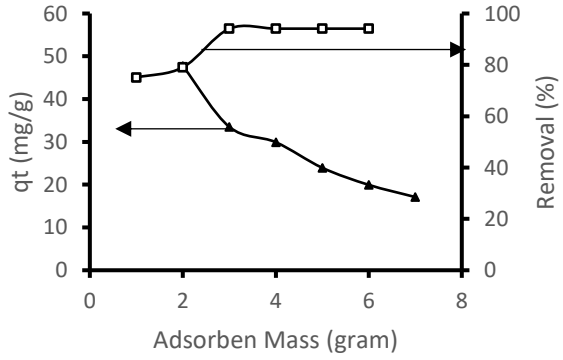

Fig. 5. Percentage removal/adsorption of Fe metal using activated carbon prepared by microwave

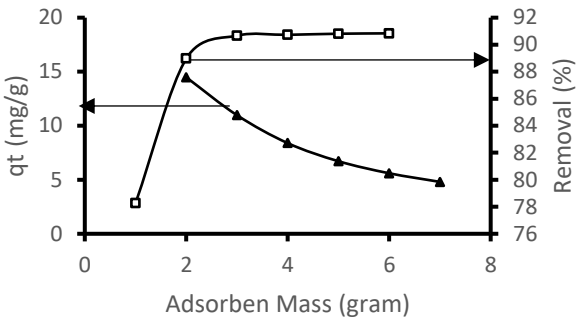

Fig. 6. Percentage removal/adsorption of Mn metal using activated carbon prepared by microwave

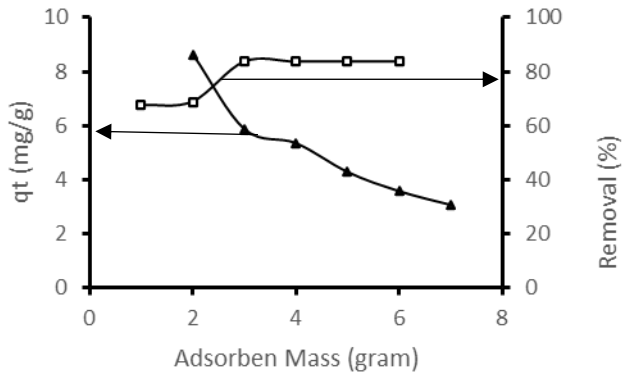

Fig. 7. Percentage removal/adsorption of Cu metal using activated carbon prepared by microwave

Figures 5, 6, and 7 indicate that with an increasing amount of adsorbent the adsorption capacity of the adsorbent also increases. This is because adding more weight of the adsorbent can lead to a higher number of particles and a larger surface area for the activated carbon. As a consequence, it can expand the overall surface area of the adsorbent. As the mass of the adsorbent rises, the percentage of adsorption also rises. This is attributed to the concurrent increase in adsorption sites or surface area along with the weight of the adsorbent, resulting in a higher percentage of metal removal at higher doses of the adsorbent. This correlation holds true for capacity values: the greater the mass of the adsorbent, the lower the adsorption capacity, and the percentage removal of metals increases correspondingly. The AAS test results indicated that, in accordance with the BET-BJH findings, a larger surface area production resulted in a higher amount of adsorbate content adhering to the surface of the carbon. Therefore, the activation, which assists microwaves, can potentially increase the adsorption of Mn, Cu, and Fe metals from acid mine waste, following [57,58]. A larger surface area of activated carbon leads to a greater adsorbate adsorption capacity. Microwave heating, in particular, enhances the synthesis of activated carbon with increased surface area and porosity, consequently facilitating higher adsorbate adsorption [59].

3.5. Contact time effect

Contact time refers to the duration over which the adsorption process occurs, reaching equilibrium when the number of impacts stabilizes. To investigate the impact of time on metal ion adsorption from acid mining waste, experiments were conducted at time intervals of 15, 30, 45, 60, 75, and 90

minutes, using a 4-gram mass. Figure 8 displays the adsorption profile of acid mine drainage at these different time points. The results revealed a progressive increase in adsorption capacities for Fe, Cu, and Mn with equilibrium reached within 60 minutes. Subsequently, there were no significant fluctuations in the concentration of metal ions. Within the initial 60 minutes, the adsorption capacities were measured at 29.9 mg/g for Fe, 1.4 mg/g for Cu, and 8.9 mg/g for Mn.

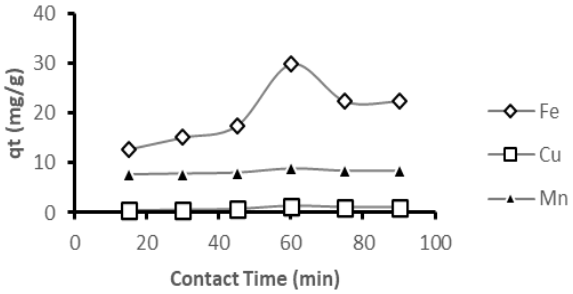

Fig. 8. Graph depicting the relationship between contact time (in minutes) and the adsorption capacity of metal ions using ACLDP

3.6. Adsorption isotherm

The adsorption of manganese (Mn), copper (Cu), and iron (Fe) from artificial acid mine waste by *Lansium domesticum* peel was evaluated using the Langmuir and Freundlich adsorption isotherm models, with the results presented in Tables 3 and 4.

Table 3. The Langmuir equations applied to the adsorption process for the metals iron (Fe), manganese (Mn), and copper (Cu)

Metal	Langmuir Isotherm		
	q_{max} (mg/g)	K_L (mol/L)	R^2
Fe	47.72	76.68	0.987934
Mn	14.52	76.65	0.963293
Cu	8.61	77.11	0.982331

Table 4. The Freundlich equations utilized to describe the adsorption process for the metals iron (Fe), manganese (Mn), and copper (Cu)

Based on the data presented in Tables 4 and 5, it is evident that the Langmuir adsorption isotherm outperformed the Freundlich model. According to the Langmuir adsorption model, the activated carbon derived from *Lansium domesticum* peel waste exhibited the maximum capacities of 14.52 mg/g, 8.61 mg/g, and 47.72 mg/g for manganese (Mn), copper (Cu), and iron (Fe) metals, respectively. This indicated that the outer layer of the activated carbon reached its saturation point in terms of adsorption capacity, making it unable to adsorb additional metal molecules. Furthermore, it is noteworthy that the concentration of the metal-containing waste solution directly impacts the number of molecules colliding with the adsorbent and subsequently interacting with it [60]. The adsorption power can be affected by the adsorbent's porosity.

In the Freundlich isotherm model, the presence of a 0 1/n1 value suggests that the adsorption is both favorable and cooperative at the same time [61,62]. According to the calculation results as shown in Table 4 [63], all 1/n values were below 0 implying that when a chemical process involves the adsorption of activated carbon from agricultural waste, the Langmuir adsorption isotherm model is a better fit. Additionally, the correlation coefficient's R^2 value is closer to 1 in the Langmuir model than in the Freundlich model.

3.7. Adsorption kinetics

The application of adsorption kinetics seeks to explore how the adsorption capacity evolves over time. This serves as a basis for constructing an engineering process model and provides valuable insights into the sorption mechanism [64]. Kinetic studies were carried out at different time intervals to better understand how the adsorption process worked. This process could be broken down into three distinct stages: first, the adsorbate moved from the bulk solution to the surface of the adsorbent, either through mass penetration or external boundary layer phenomena; second, the adsorbate migrated into the active sites by passing through the pores, referred to as pore diffusion or intraparticle diffusion; and finally, the adsorbate was adsorbed onto the surface through physical or chemical reactions [65]. The analysis of adsorption kinetics modeling involved assessing both pseudo-first-order and pseudo-second-order models.

The equation that represents the pseudo-first-order (PFO) or Lagergren model can be expressed as follows [66]:

$$\ln(q_e - q_t) = \ln (q_e - k_1 t) \quad (4)$$

This model involves parameters like qe and qt, measured in milligrams per gram (mg/g), which signify the adsorption capacities at equilibrium and at a specific time t, expressed in minutes (min). Furthermore, k_1 represents the rate constant for

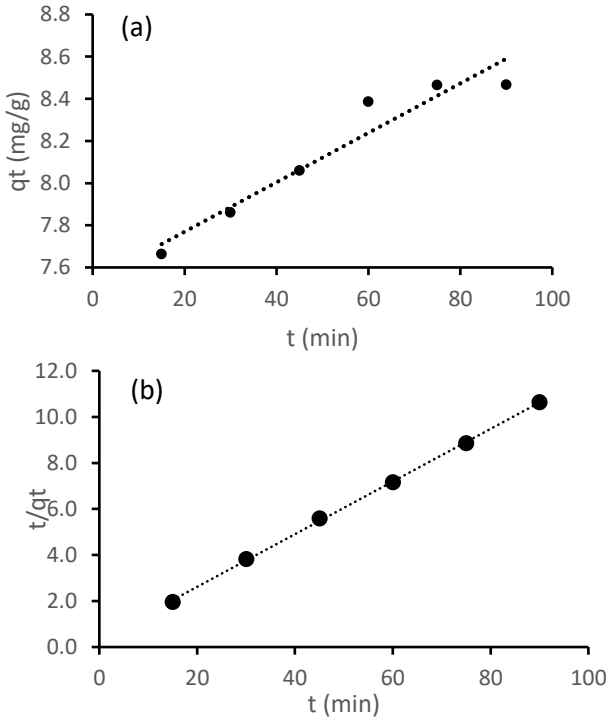

Fig. 9. Plot of (a) PFO adsorption process for Mn; (b) PSO adsorption process for Mn

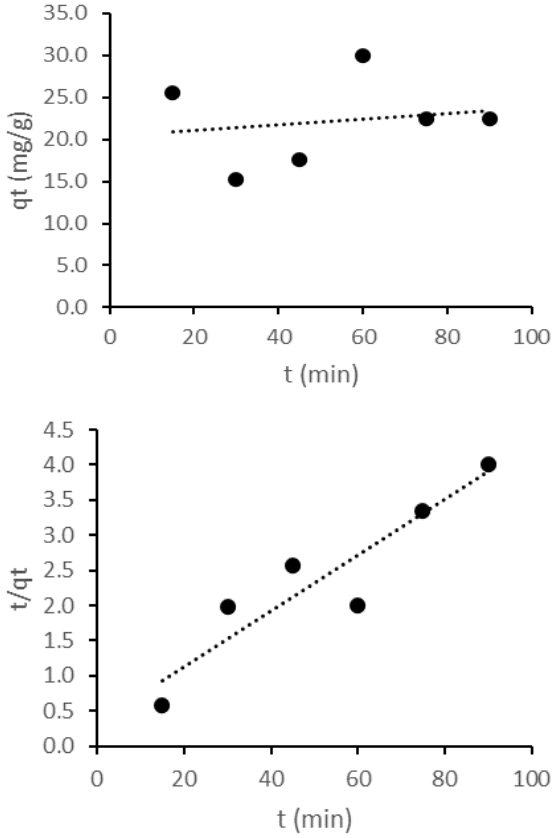

Fig. 10. Plot of (a) PFO adsorption process for Cu; (b) PSO adsorption process for Cu

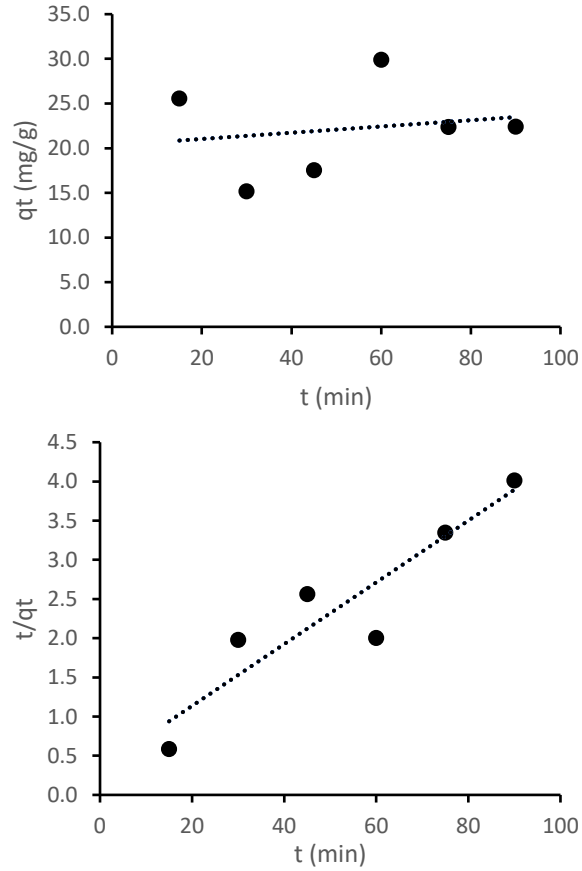

Fig. 11. Plot of (a) PFO adsorption process for Fe; (b) PSO adsorption process for Fe

the pseudo-first-order (PSO) adsorption process, measured in units of 1/min. Figures 9(a), 10(a), and 11(a) depict the graphical representations of the pseudo-first-order (PFO) kinetic plots for the removal of Mn, Cu, and Fe ions through the use of ACLDP representing for the removal of Mn, Cu, and Fe ions through the use of ACLDP.

The equation representing the pseudo-second order (PSO) or Lagergren [67] model is presented as follows:

$$\frac{1}{q_t} = \frac{1}{k_2 q_e^2} + \frac{t}{q_e} \quad (5)$$

This graph encompasses various parameters: qe and qt, denoting the amount of metal adsorbed onto the adsorbent, measured in milligrams per gram (mg/g), both at equilibrium and at a specific time t, respectively. It also involves the rate constant k_2, expressed in the units of g/mg·min. Figures 9(b), 10(b), and 11(b) provide the graphical representations of the pseudo-second-order kinetic plots illustrating the removal of Mn, Cu, and Fe ions through the use of ACLDP. Table 5 presents the obtained parameters for the kinetics Fe, Cu and Mn ions adsorption on ACLDP.

Table 5. The adsorption kinetics of Fe, Cu, and Mn ions on ACLDP

Kinetics Model	Metals	Parameters	Value
Pseudo-First-Order (PFO)	Fe	q_e (mg/g)	29.9166
		k_1 (min^{-1})	76.6857
		R^2	0.9186
	Mn	q_e (mg/g)	8.3870
		k_1 (min^{-1})	76.5878
		R^2	0.9605
	Cu	q_e (mg/g)	29.9166
		k_1 (min^{-1})	76.6857
		R^2	0.9186
Pseudo-Second-Order (PSO)	Fe	q_e (mg/g)	2.0056
		k_2 (g $mg^{-1}min^{-1}$)	83.2347
		R^2	0.9516
	Mn	q_e (mg/g)	7.1539
		k_2 (g $mg^{-1}min^{-1}$)	15.4304
		R^2	0.9390
	Cu	q_e (mg/g)	2.0056
		k_2 (g $mg^{-1}min^{-1}$)	83.2347
		R^2	0.9516

The findings revealed that there was a considerable degree of similarity in the outcomes obtained from both the PFO and PSO models for the adsorption of all the metals [68], although there was still a minor discrepancy that was not highly significant (R^2= 0.9516; 0.9390; 0.9516) for PSO and for PFO (R^2= 0.9186; 0.9605; 0.9186). PFO suggested a tendency toward physisorption, while PSO was associated with electron transfer or ion exchange, indicating chemisorption between the adsorbent and adsorbate [69]. Physisorption is characterized by weak van der Waals forces that diminish as the temperature increases. On the other hand, chemisorption entails the creation of chemical bonds, requiring activation energy, and, akin to various chemical reactions, enhanced by an increase in temperature. In physical adsorption, the multilayers of adsorbed particles are formed but in chemical adsorption, monolayer of adsorbed particles is formed**.** This chemisorption process aligned with previous studies on agricultural waste

[70–72]. The proximity of the coefficient of regression (R^2) to unity (1) [73–75] was employed to assess how well the determined model suited the data, so as a result, the predicted R^2 values from the PSO model matched well with the experimental values. This is also in line with the research findings that the data follows Langmuir isotherm adsorption (monolayer).

4. Conclusion

This research aims to explore the feasibility of using agricultural waste, specifically *Lansium domesticum* peel, as an economical sorbent for heavy metals through the application of isothermal models with microwave-assisted activation. Characterization results confirmed that the activated carbon derived from Lansium domesticum peel at 400 watts exhibited a substantial carbon content and a more extensive, clean, and smoother pore structure along with the increased porosity and pore size. The activation time was relatively shorter, i.e. 10 minutes. The BET surface area reached 1367.0385 m2/g, the mesoporous size was 2.25 nm, the average pore diameter was 4V/A, and the BJH adsorption cumulative volume was 1.112 cm3/g. Working parameters such as initial concentration, biosorbent dosage, and contact time were analyzed and obtained influence the sorption efficiency of activated carbon. The adsorption process of activated carbon derived from *Lansium domesticum* peel follows a second-order rate law, where the mechanism of the adsorption process is chemisorption. In the context of removing Mn, Cu, and Fe metals from acid mine waste, activated carbon demonstrated remarkable efficiency, as evaluated using the Langmuir adsorption model. The removal efficiencies were 94.08% for Fe, 90.67% for Mn, and 83.69% for Cu. Indicating a superior fit of the adsorption isotherm curve to the Langmuir model. These findings underscored the potential of ACLDP as a promising and cost-effective adsorbent with impressive adsorption capabilities for effectively eliminating Fe, Cu, and Mn from wastewater.

Acknowledgements

The authors received a Grant-in-Aid for Scientific Research from the Ministry of Research, Technology, and Higher Education, Number: B/67/D. D3/KD.02.00/2019, to apply for BPPDN (Beasiswa Pendidikan Pascasarjana Dalam Negeri or the Domestic Postgraduate Education Scholarship) in 2019.

References

1. E. W. M. Verheij, *Plant resource of South-East Asia: edible fruits and nuts*, No.2, Edible Fruits and Nuts. Prosea Foundation, Bogor, Indonesia, 1992.
2. O. A. Saputra, Kurnia, S. Pujiasih, V.N. Rizki, B. Nurhayati, E. Pramono, and C. Purnawan, *Silylated-montmorillonite as co-adsorbent of chitosan composites for methylene blue dye removal in aqueous solution*, Commun. Sci. Technol. 5 (2020) 45–52.
3. A. A. Ojo, I. Osasona, A.O. Olawole, and J. A. Johnson, *Acid And Bio-Activation Of Carbon Prepared From Corncob For Adsorption Of Cd(II) From Aqueous Solution*, Rasayan J. Chem. 15 (2022), 889–893.
4. G. Sharma, S. Sharma, A. Kumar, C. W. Lai, M. Naushad, Shehnaz, J. Iqbal, and F. J. Stadler, *Activated Carbon as Superadsorbent and Sustainable Material for Diverse Applications*, Adsorpt. Sci. Technol. 20 (2022) 1-21.
5. M. Rahmayanti, A. Yahdiyani, and I. Q. Afifah, *Eco-friendly synthesis of magnetite based on tea dregs (Fe3O4-TD) for methylene blue adsorbent from simulation waste,* Commun. Sci. Technol. 7 (2022) 119–126.
6. A. Demba N'diaye, M. Sid'Ahmed Kankou, B. Hammouti, A. B. D. Nandiyanto, and D. F. Al Husaeni, *A review of biomaterial as an adsorbent: From the bibliometric literature review, the definition of dyes and adsorbent, the adsorption phenomena and isotherm models, factors affecting the adsorption process, to the use of typha species waste as a low-cost*, Commun. Sci. Technol. 7 (2022) 140–153.
7. E. M. Mistar, T. Alfatah, and M. D. Supardan, S*ynthesis and characterization of activated carbon from Bambusa vulgaris striata using two-step KOH activation*, J. Mater. Res. Technol. 9 (2020) 6278–6286.
8. I. Syauqiah, D. Nurandini, N. S. Prihatini, and J. Jamiyaturrasidah, *Kinetic Studies Of Cu Adsorption From Sasirangan Liquid Waste Using Rice Husk Activated Carbon*, Konversi, 10 (2021) 115–119.
9. A. S. K. Harivram, I. Syauqiah, M. Elma, E. L. A. Rampun, D. A. C. Putri, and N. G. Safitri, *Iron Adsorption In Peat Water By Sago Waste Activated Carbon*, Konversi, 11 (2022), 64–68.
10. Y. Gomez-Rueda, B. Verougstraete, C. Ranga, E. Perez-Botella, F. Reniers, and J. F. M. Denayer, *Rapid temperature swing adsorption using microwave regeneration for carbon capture*, Chem. Eng. J., 446 (2022) 1-13.
11. E. Kocbek, H. A. Garcia, C. M. Hooijmans, I. Mijatović, B. Lah, and D. Brdjanovic, *Microwave treatment of municipal sewage sludge: Evaluation of the drying performance and energy demand of a pilot-scale microwave drying system*, Sci. Total Environ. 742 (2020) 1-13.
12. Y. Mao, J. Robinson, and E. Binner, *Understanding heat and mass transfer processes during microwave-assisted and conventional solvent extraction*, Chem. Eng. Sci. 233 (2021) 1-13.
13. W. Tayier, S. Janasekaran, and V. C. Tai, *Microwave hybrid heating (MHH) of Ni-based alloy powder on Ni and steel-based metals –A review on fundamentals and parameters*, Int. J. Light. Mater. Manuf. 5 (2022), 58–73.
14. P. Mukwevho, and M. N. Emmambux, *Effect of infrared and microwave treatments alone and in combination on the functional properties of resulting flours from bambara groundnut seeds*, LWT. 153 (2022) 1-10.
15. J. Tang, and F. P. Resurreccion, *Electromagnetic basis of microwave heating*, *Dev. Packag. Prod. Use Microw. Ovens*, Woodhead Publishing Ltd. 2009.
16. V. Palma, D. Barba, M. Cortese, M. Martino, S. Renda, and E. Meloni, *Microwaves and heterogeneous catalysis: A review on selected catalytic processes*, Catalysts, 10 (2020) 1-58 .
17. L. Kistriyani, Z. Salimin, and A. Chafidz, *Utilization of extracellular polymeric substances (EPS) immobilized in epoxy polymer as double ion exchanger biosorbent for removal of chromium from aqueous solution*, Commun. Sci. Technol., 5 (2020), 40–44.
18. S. Cheng, S. Zhang, L. Zhang, H. Xia, J. Peng, and S. Wang, *Microwave-Assisted Preparation of Activated Carbon from Eupatorium Adenophorum: Effects of Preparation Parameters*, High Temp. Mater. Process. 36 (2017) 805–814.
19. S. Zhang, S. Liu, D. Yu, C. Wang, and Q. Li, *Preparation and characterization of activated carbon for separation of CO2*, Zhongguo Kuangye Daxue Xuebao/Journal China Univ. Min. Technol. 43 (2014), 910–914.
20. A. Nur Hidayah, M. A. Umi Fazara, Z. Nor Fauziah, and M. K. Aroua,

Preparation and characterization of activated carbon from the sea mango (Cerbera Odollam) with impregnation in phosphoric acid (H3PO4), Asean J. Chem. Eng. 15 (2015) 22–30.

21. G. Enaime, K. Ennaciri, A. Ounas, A. Baçaoui, M. Seffen, T. Selmi, and A. Yaacoubi, *Preparation and characterization of activated carbons from olive wastes by physical and chemical activation: Application to Indigo carmine adsorption*, J. Mater. Environ. Sci. 8 (2017) 4125–4137.
22. M. Zięzio, B. Charmas, K. Jedynak, M. Hawryluk, and K. Kucio, *Preparation and characterization of activated carbons obtained from the waste materials impregnated with phosphoric acid(V)*, Appl. Nanosci. 10 (2020) 4703–4716.
23. H. Fałtynowicz, J. Kaczmarczyk, and M. Kułazyński, *Preparation and characterization of activated carbons from biomass material - Giant knotweed (Reynoutria sachalinensis)*, Open Chem., 13 (2015) 1150–1156.
24. O.A., Ekpete, and JNR, Horsfall., *Preparation and Characterization of Activated Carbon Derived From Fluted Pumpkin Stem Waste (Telfairia Occidentalis Hook . F),* Res. J. Chem. Sci. 1 (2011) 10-17.
25. D. O. Kra, N. B. Allou, P. Atheba, P. Drogui, and A. Trokourey, *Preparation and Characterization of Activated Carbon Based on Wood*, J. Encapsulation Adsorpt. Sci. 9 (2019), 63–82.
26. K. V. Kumar, S. Gadipelli, B. Wood, K. A. Ramisetty, A. A. Stewart, C. A. Howard, D. J. L. Brett, and F. Rodriguez-Reinoso, *Characterization of the adsorption site energies and heterogeneous surfaces of porous materials*, J. Mater. Chem. 7 (2019) 10104–10137.
27. R. Chen, L. Li, Z. Liu, M. Lu, C. Wang, H. Li, W. Ma, and S. Wang, *Preparation and characterization of activated carbons from tobacco stem by chemical activation*, J. Air Waste Manag. Assoc. 67 (2017) 713–724.
28. A. H. Abdullah, A. Kassim, Z. Zainal, M. Z. Hussien, and F. A. Dzulkefly Kuang, *Preparation and Characterization of Activated Carbon from Gelam Wood Bark (Melaleuca cajuputi)*, Malaysian J. Anal. Sci. 7 (2001) 65–68.
29. D. Das, D. P. Samal, and BC. Meikap, *Preparation of Activated Carbon from Green Coconut Shell and its Characterization*, J. Chem. Eng. Process Technol., 6 (2015) 1-7.
30. J. Yuan, Z. Ding, Y. Bi, J. Li, S. Wen, and S. Bai, *Resource Utilization of Acid Mine Drainage (AMD): A Review*, Water (Switzerland), 14 (2022) 1–15.
31. R. Mohadi, N. R. Palapa, T. Taher, P. M. S. B. N. Siregar, Normah, N. Juleanti, A. Wijaya, and A. Lesbani, *Removal of Cr(VI) from aqueous solution by biochar derived from rice husk*, Commun. Sci. Technol., 6 (2021) 11–17.
32. N. S. Prihatini, B. J. Priatmadi, A. Masrevaniah, and S. Soemarno, *Performance of The Horizontal Subsurface-Flow Constructed Wetland with Different Operational Procedures*, Int. J. Adv. Eng. Technol., 7 (2015) 1620–1629.
33. Z. Hu, X. Ma, and C. Chen, *A study on experimental characteristic of microwave-assisted pyrolysis of microalgae*, Bioresour. Technol. 107 (2012) 487–493.
34. A. B. D. Nandiyanto, G. C. S. Girsang, R. Maryanti, R. Ragadhita, S. Anggraeni, F. M. Fauzi, P. Sakinah, A. P. Astuti, D. Usdiyana, M. Fiandini, M. W. Dewi, and A. S. M. Al-Obaidi, *Isotherm adsorption characteristics of carbon microparticles prepared from pineapple peel waste*, Commun. Sci. Technol. 5 (2020) 31–39.
35. W. S. Chen, Y. C. Chen, and C. H. Lee, Modified Activated Carbon for Copper Ion Removal from Aqueous Solution, *Processes*, 10 (2022) 1-16.
36. N. Ayawei, A. N. Ebelegi, and D. Wankasi, *Modelling and Interpretation of Adsorption Isotherms*, J. Chem. 136 (2017) 1-11.
37. S. Kumar, Carbon based nanomaterial for removal of heavy metals from wastewater: a review, *Int. J. Environ. Anal. Chem.*, 103 (2021) 1–18.
38. C. Bommier, R. Xu, W. Wang, X. Wang, D. Wen, J. Lu, and X. Ji, *Self-activation of cellulose: A new preparation methodology for activated carbon electrodes in electrochemical capacitors*, Nano Energy. 13 (2015) 709–717.
39. S. Maulina, G. Handika, Irvan, and A. H. Iswanto, *Quality comparison of activated carbon produced from oil palm fronds by chemical activation using sodium carbonate versus sodium chloride*, J. Korean Wood Sci. Technol. 48 (2020) 503–512.
40. S. Basu, G. Ghosh, and S. Saha, *Adsorption characteristics of phosphoric acid induced activation of bio-carbon: Equilibrium, kinetics, thermodynamics and batch adsorber design*, Process Saf. Environ. Prot. 117 (2018) 125–142.
41. D. Duan, Y. Zhang, Y. Wang, H. Lei, Q. Wang, and R. Ruan, *Production of renewable jet fuel and gasoline range hydrocarbons from catalytic pyrolysis of soapstock over corn cob-derived activated carbons*, Energy, 209 (2020) 1-12.
42. S. M. Yakout, and G. Sharaf El-Deen, *Characterization of activated carbon prepared by phosphoric acid activation of olive stones*, Arab. J. Chem. 9 (2016) S1155–S1162.
43. P. M. Álvarez, F. J. Beltrán, V. Gómez-Serrano, J. Jaramillo, and E. M. Rodríguez, *Comparison between thermal and ozone regenerations of spent activated carbon exhausted with phenol*, Water Res. 38 (2004) 2155–2165.
44. E. F. Jaguaribe, L. L. Medeiros, M. C. S. Barreto, and L. P. Araujo, *The performance of activated carbons from sugarcane bagasse, babassu, and coconut shells in removing residual chlorine*, Brazilian J. Chem. Eng. 22 (2005) 41–47.
45. M. Sudibandriyo, and F. A. Putri, *The Effect of Various Zeolites as an Adsorbent for Bioethanol Purification using a Fixed Bed Adsorption Column,* Int. J. Technol. 11 (2020) 1300–1308.
46. L. Ni'Mah, M. F. Setiawan, and S. P. Prabowo, *Utilization of Waste Palm Kernel Shells and Empty Palm Oil Bunches as Raw Material Production of Liquid Smoke*, IOP Conf. Ser. Earth Environ. Sci. 366 (2019) 1-9.
47. D. Bergna, T. Varila, H. Romar, and U. Lassi, *Activated carbon from hydrolysis lignin: Effect of activation method on carbon properties*, Biomass and Bioenergy. 159 (2022) 1-8.
48. K. Y. Foo, *Effect of microwave regeneration on the textural network, surface chemistry and adsorptive property of the agricultural waste based activated carbons*, Process Saf. Environ. Prot., 116 (2018) 461–467.
49. X. Liu, C. Sun, H. Liu, W. H. Tan, W. Wang, and C. Snape, C., *Developing hierarchically ultra-micro/mesoporous biocarbons for highly selective carbon dioxide adsorption*, Chem. Eng. J., 361 (2019) 199–208.
50. S. Cheng, L. Zhang, H. Xia, J. Peng, S. Zhang, and S. Wang, *Preparation of high specific surface area activated carbon from walnut shells by microwave-induced KOH activation*, J. Porous Mater. 22 (2015) 1527–1537.
51. R. Hoseinzadeh Hesas, W. M. A. Wan Daud, J. N. Sahu, and A. Arami-Niya, *The effects of a microwave heating method on the production of activated carbon from agricultural waste: A review*, J. Anal. Appl. Pyrolysis. 100 (2013) 1–11.
52. C. Cheng, H. Liu, P. Dai, X. Shen, J. Zhang, T. Zhao, and Z. Zhu, *Microwave-assisted preparation and characterization of mesoporous activated carbon from mushroom roots by phytic acid (C6H18O24P6) activation*, J. Taiwan Inst. Chem. Eng. 67 (2016) 532–537.
53. F. Mbarki, T. Selmi, A. Kesraoui, M. Seffen, P. Gadonneix, A. Celzard, and V. Fierro, *Hydrothermal pre-treatment, an efficient tool to improve activated carbon performances*, Ind. Crops Prod. 140 (2019) 1-40.
54. A. M. Abioye, and F. N. Ani, *The Characteristics of Oil Palm Shell Biochar and Activated Carbon Produced via Microwave Heating*, Appl. Mech. Mater. 695 (2014) 12–15.
55. A. Kundu, *Advancement of Adsorption Process on Activated Carbon Using Mocrowave and High Gravimetric Technologies*, Ph.D. Thesis,

University of Malaya, Malaysia, 2016.

56. C. Liu, W. Chen, S. Hong, M. Pan, M. Jiang, Q. Wu, and C. Mei, *Fast microwave synthesis of hierarchical porous carbons from waste palm boosted by activated carbons for supercapacitors*, Nanomaterials, 9 (2019) 1-13.
57. M. Danish, J. Birnbach, M. N. Mohamad Ibrahim, R. Hashim, S. Majeed, G. S. Tay, and N. Sapawe, *Optimization study of caffeine adsorption onto large surface area wood activated carbon through central composite design approach*, Environ. Nanotechnology, Monit. Manag. 16 (2021) 1-10.
58. A. Kumar, C. Patra, S. Kumar, and S. Narayanasamy, *Effect of magnetization on the adsorptive removal of an emerging contaminant ciprofloxacin by magnetic acid activated carbon*, Environ. Res., 206 (2022) 1-11.
59. M. F. Zulkornain, A. H. Shamsuddin, S. Normanbhay, J. Md Saad, Y. S. Zhang, S. Samsuri, and W. A. Wan Ab Karim Ghani, Microwave-assisted Hydrothermal Carbonization for Solid Biofuel Application: A Brief Review, *Carbon Capture Sci. Technol.*, 1 (2021) 1-14.
60. N. K. Soliman, and A. F. Moustafa, *Industrial solid waste for heavy metals adsorption features and challenges; a review*, J. Mater. Res. Technol. 9 (2020) 10235–10253.
61. P. Thirupathi, and B. R. Venkatraman, *Corrosion Kinetic And Adsorption Thermodynamic Activity Of Enicostemma Littorale (Indian Whitehead) For Carbon Steel In Well Water*, Rasayan J. Chem. 15 (2022) 1757–1771.
62. N. Minh Dat, L. Minh Huong, N. Tien Dat, D. Ba Thinh, D. Ngoc Trinh, N. Thi Huong Giang, M. Thanh Phong, and N. Huu Hieu, *Synthesis of hygroscopic sodium alginate-modified graphene oxide: Kinetic, isotherm, and thermodynamic study*, Eur. Polym. J. 174 (2022) 1-11.
63. A. A. Ahmad, M. A. Ahmad, N. K. E. M. Yahaya, and J. Karim, *Adsorption of malachite green by activated carbon derived from gasified Hevea brasiliensis root*, Arab. J. Chem. 14 (2021) 1-13.
64. An, Byungryul, C*u(II) and As(V) adsorption kinetic characteristic of the multifunctional amino groups in chitosan*, Processes. 8 (2020) 1-15.
65. E. El Qada, *Kinetic Behavior of the Adsorption of Malachite Green Using Jordanian Diatomite as Adsorbent*, Jordanian J. Eng. Chem. Ind. 3 (2020) 1–10.
66. S. H. Yuh, *Citation review of Lagergren kinetic rate equation on adsorption reactions*, Scientometrics. 59 (2004) 171–177.
67. Y. S. Ho, *Adsorption Of Heavy Metals From Waste Streams By Peat,* Ph.D Thesis, The University of Birmingham, 1995.
68 F. Mbarki, T. Selmi, A. Kesraoui, and M. Seffen, *Low-cost activated carbon preparation from Corn stigmata fibers chemically activated using H3PO4, ZnCl2 and KOH: Study of methylene blue adsorption, stochastic isotherm and fractal kinetic,* Ind. Crops Prod. 178 (2022) 1-16.
69. M. Belhachemi, and F. Addoun, *Comparative adsorption isotherms and modeling of methylene blue onto activated carbons*, Appl. Water Sci. 1 (2011) 111–117.
70. K. Banerjee, *A Novel Agricultural Waste Adsorbent, Watermelon Shell for the Removal of Copper from Aqueous Solutions*, Iran. J. Energy Environ. 3 (2012) 143–156.
71. A. Witek-Krowiak, and D. Harikishore Kumar Reddy, *Removal of microelemental Cr(III) and Cu(II) by using soybean meal waste – Unusual isotherms and insights of binding mechanism*, Bioresour. Technol. 127 (2013) 350–357.
72. N. R. Palapa, A. F. Badri, Mardiyanto, R. Mohadi, T. Taher, and A. Lesbani, *Mg/Cr-(COO)22- layered double hydroxide for malachite green removal,* Commun. Sci. Technol. 7 (2022) 91–97.
73. P. M. S. B. N. Siregar, Normah, N. Juleanti, A. Wijaya, N. R. Palapa, R. Mohadi, and A. Lesbani, *Mg/Al-CH, Ni/Al-CH, and Zn/Al-CH as adsorbents for Congo Red removal in aqueous solution*, Commun. Sci. Technol. 6 (2021) 74–79.
74. D. I. Lestari, A. T. Yuliansyah, and A. Budiman, *Adsorption studies of KOH-modified hydrochar derived from sugarcane bagasse for dye removal: Kinetic, isotherm, and thermodynamic study*, Commun. Sci. Technol. 7 (2022) 15–22.
75. D. R. Wicakso, A. Mirwan, E. Agustin, N. F. Nopembriani, I. Firdaus, and M. Fadillah, *Potential of silica from water treatment sludge modified with chitosan for Pb(II) and color adsorption in sasirangan waste solution,* Commun. Sci. Technol. 7 (2022) 188–193.